CORROSION AND TENSILE TESTING STUDY OF HIGH TEMPERATURE AND HIGH PRESSURE WELL INJECTION AND PRODUCTION INTEGRATED STRING

by

Hongzhi SONG[a], Wei MEI[a*], Jianliang ZHANG[a], Weihong LONG[a], and Hongchuan ZHAO[b]

[a] China Oilfield Services Limited (COSL), Tianjin, China
[b] MOE Key Laboratory of Petroleum Engineering, China University of Petroleum, Beijing, China

Original scientific paper
https://doi.org/10.2298/TSCI2404567S

In this study, corrosion experiments were conducted on three commonly used materials for integrated strings (L80, 2205, P110) using the hanging strip corrosion method at high temperature and high pressure. Subsequently, high temperature tensile tests were performed on the three materials, and the variations in parameters such as corrosion rate, yield strength, and tensile strength under different experimental temperatures were compared and analyzed. The experimental results indicate that with increasing experimental temperature, the corrosion rate of all three materials shows an upward trend, while the yield strength and tensile strength exhibit a decreasing trend. The P110 material not only has the highest yield strength but also the lowest corrosion rate under different environmental temperatures, demonstrating better material characteristics in the operating environment.

Key words: *heavy oil, thermal recovery wells, corrosion experiments, integrated injection-production strings,*

Introduction

Steam-assisted recovery technology quickly enhances heavy oil flowability by injecting high pressure steam into reservoirs through integrated injection-production strings. These strings endure harsh conditions, including high temperature, pressure, and corrosive fluids, leading to frequent failures and economic losses. Corrosion experiments typically use gravimetric, electrochemical, and surface analysis methods [1, 2]. Hanging strip corrosion is widely used for studying average corrosion rates, while electrochemical techniques assess corrosion resistance [3-5]. Corrosion product analysis examines microscopic morphology and composition [6]. Despite progress in predicting corrosion life, challenges remain due to the complex structure and harsh conditions of integrated injection-production strings. Thus, this study conducted corrosion experiments on commonly used materials (L80, 2205, P110) and subsequent tensile tests to provide guidance for optimizing design and safety evaluation.

* Corresponding author. e-mail: meiwei@cnooc.com.cn

Experimental materials and methods

Corrosion experiment

The experimental materials consisted of three commonly used materials for integrated injection-production strings: L80 steel, P110 steel, and 2205 stainless steel. The preparation of experimental specimens followed the method outlined in JB/T 7901-1999 *Method for Uniform Corrosion Immersion Test of Metal Materials* with specimens sized at 50 mm × 10 mm × 3 mm hanging strips. Prior to the experiment, each specimen was sequentially polished using 320#, 600#, and 1200# sandpaper to remove oxidation and physical irregularities. They were then cleaned with deionized water, degreased with acetone, and dehydrated with anhydrous ethanol. The dimensions (length, width, thickness, and aperture) of each specimen were measured, and their masses were recorded before the experiment. Subsequently, the specimens were insulated from each other and mounted on a specially designed test rack, which was placed into the experimental medium within a high pressure autoclave (see tab. 1 for medium composition). High purity nitrogen gas was first introduced for two hours to remove oxygen, followed by the introduction of high purity CO_2 and O_2, and then nitrogen was introduced to reach the desired pressure. The experiment was conducted at temperatures of 120 °C and 240 °C, with a working pressure set at 18 MPa inside the high temperature and high pressure reaction vessel. The partial pressures of each component are presented in tab. 1. The experimental period lasted for 72 hours, with each material undergoing three parallel tests. The principle and process of the corrosion experiment are illustrated in fig. 1. After completion of the experiment, the specimens were removed from the autoclave, rinsed with distilled water to remove dissolved salts from the surface, dehydrated with anhydrous ethanol, air-dried, and finally weighed to determine the post-corrosion mass. All reagents used in the experiment were of analytical grade.

Table 1. Simulation of the partial pressures of various components of downhole multi-phase hot fluids

Components	Pressures
CO_2	0.55 MPa
O_2	0.04 MPa
N_2	2.08 MPa
H_2O	15.33 MPa

Tensile test

The experimental materials consisted of L80 steel, P110 steel, and 2205 stainless steel. The dimensions of the tensile test specimens are as shown in fig. 2.

Table 2. The dimensions of the tensile specimen [mm]

A	*B*	*C*	*D*	*G*	*L*
30	20	20	6.25	25	70

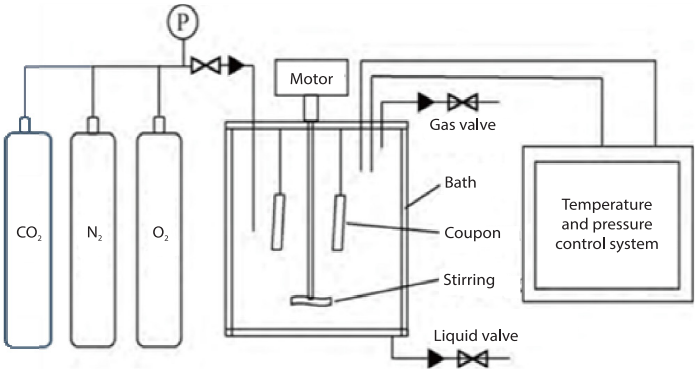

Figure 1. High temperature and high pressure corrosion test apparatus diagram

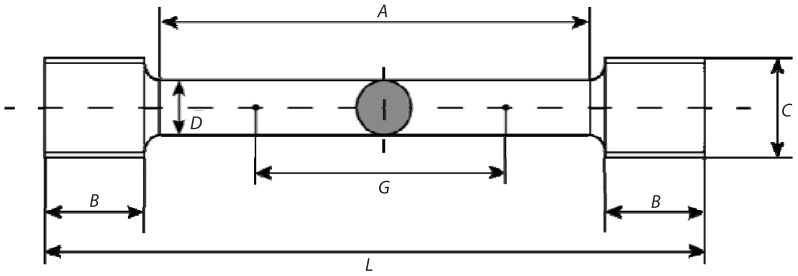

Figure 2. Schematic diagram of tensile specimen

Development of a conjugal transfer system

The tensile testing equipment used was the Z100HT electronic universal materials testing machine, manufactured by Zwick GmbH, Germany. It was equipped with a 900 °C high temperature furnace, high temperature grips, and a high temperature extensometer. This set-up could meet the testing requirements for room temperature and high temperature tensile tests ranging from 100-900 °C. The tensile tests followed the specifications outlined in ASTM E21-20. The diameter of the tensile test specimens was 6.25 mm, with a gauge length of 25 mm, as shown in fig. 2. The tensile tests were conducted in a high temperature environment provided by the high temperature furnace. The test specimens were placed inside the furnace and clamped using high temperature grips. The tensile rate was controlled using a beam displacement method, with the magnitude determined by the parallel length and strain rate. The strain rate was set at 0.005 per minute before yielding and 0.05 per minute after yielding until specimen failure, with a strain of 1% designated as the speed switching point. The heating temperature of the specimens was maintained at 120 °C and 240 °C, with a dwell time of 15 minute and 20 minute, respectively.

Results and analysis

Corrosion test results

The morphologies of the three materials before and after corrosion at different temperatures are shown in figs. 3 and 4. When the temperature of the corrosion test environment was 120 °C, a reddish-brown corrosion product appeared on the surfaces of the corrosion coupons of all three materials after the corrosion test. Among them, the L80 coupon surface had more reddish-brown corrosion products, indicating more severe corrosion, while the corrosion situation of P110 and 2205 was less severe. However, the corrosion products on the corrosion coupons of all three materials appeared to be relatively loose. When the corrosion environment temperature increased to 240 °C, after the corrosion test of the three materials' weight loss coupons, a layer of black-brown corrosion product covered the surfaces. The corrosion products were relatively dense, with some local detachment. Among them, the surfaces of the N80 and P110 coupons were extensively covered by corrosion products, indicating more severe corrosion, while the corrosion situation on the 2205 coupon surfaces was less severe. Tables 3 and 4 show the calculated uniform corrosion rates of the three materials under conditions of 120 °C and 240 °C, with a CO_2 partial pressure of 0.55 MPa. From the tables, it can be observed that at a temperature of 120 °C, the uniform corrosion rate of L80 steel was 0.0368 mm annualy, P110 steel was 0.0118 mm annualy, and 2205 stainless steel was 0.0172 mm annualy. As the corrosion environment temperature increased to 240 °C, the uniform corrosion rates all increased. Particularly, the average corrosion rate of L80 steel was the highest, reaching 0.0513 mm an-

nualy, which increased by 39% compared to the previous rate. The increase in the uniform corrosion rate of 2205 stainless steel was relatively small, only increasing by 6.3% compared to the original rate.

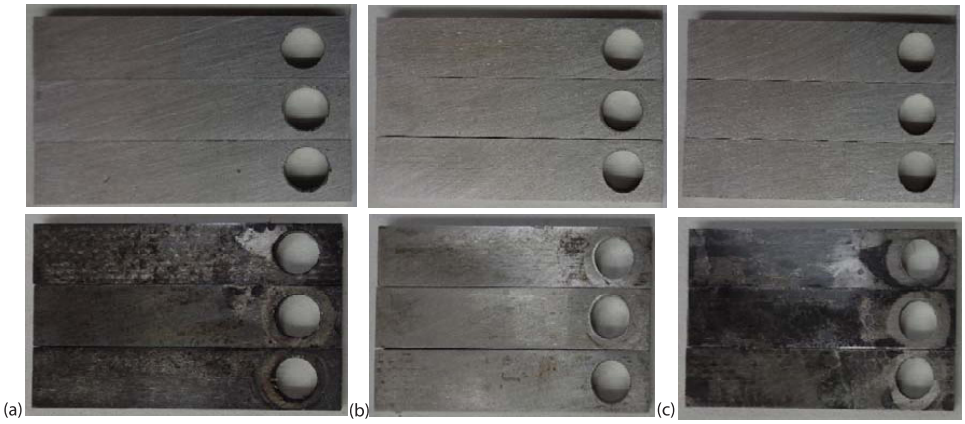

Figure 3. Comparison chart of corrosion before and after testing at 240 °C; (a) comparison of L80 before and after corrosion, (b) comparison of 2205 before and after corrosion, and (c) comparison of P110 before and after corrosion

Table 3. Calculation results of uniform corrosion rates for the three materials at 120 °C

Material	Total area [cm^2]	Initial weight [g]	Final weight [g]	Weight loss [g]	Corrosion rate [mm annualy]	Average corrosion rate [mm annualy]
L80	13.0006	10.9195	10.9165	0.0003	0.0364	0.0368
	13.0378	10.9462	10.9411	0.0052	0.0630	
	13.0153	10.9425	10.9416	0.0009	0.0109	
P110	12.9143	11.0075	11.0068	0.0007	0.0085	0.0118
	12.9338	10.9679	10.9658	0.0021	0.0256	
	12.9901	11.0766	11.0765	0.0001	0.0012	
2205	12.9729	11.0325	11.0316	0.0009	0.0105	0.0172
	12.9795	11.0859	11.0857	0.0002	0.0023	
	12.9927	11.0865	11.0832	0.0033	0.0387	

Table 4. Calculation results of uniform corrosion rates for the three materials at 240 °C

Material	Total area [cm^2]	Initial weight [g]	Final weight [g]	Weight loss [g]	Corrosion rate [mm annualy]	Average corrosion rate [mm annualy]
L80	13.0392	10.9263	10.9212	0.0051	0.0618	0.0513
	13.0380	10.9528	10.9473	0.0055	0.0667	
	13.0457	10.9501	10.9480	0.0021	0.0254	
P110	13.0406	10.9501	10.9480	0.0021	0.0254	0.0198
	13.0208	11.0625	11.0609	0.0016	0.0194	
	13.0153	11.0443	11.0431	0.0012	0.0146	
2205	13.0167	11.0136	11.0116	0.0020	0.0234	0.0183
	13.0406	11.0631	11.0619	0.0012	0.0140	
	13.0835	11.0876	11.0861	0.0015	0.0175	

Tensile test results

Figure 4 and tab. 5 depict stress-strain curves of the three materials at 120 °C and 240 °C. The elastic modulus remains relatively consistent across temperatures, with L80 exhibiting the highest at 198 GPa and 2205 the lowest at 193 GPa at 120 °C. At 240 °C, all materials show a slight decrease in elastic modulus. However, beyond the elastic limit, noticeable differences occur between the materials, with P110 displaying the highest yield strength and 2205 the lowest. As temperature increases, both yield and ultimate tensile strengths decrease for all materials. Table 6 presents yield strength and ultimate tensile strength results, with increasing temperature from 120-240 °C, material elongation generally increases while strength decreases. P110 steel exhibits the highest strength, with average yield and ultimate tensile strengths of 817 MPa and 866 MPa at 120 °C, and 773 MPa and 818 MPa at 240 °C, respectively. The L80 steel displays the highest corrosion rate at 0.0368 mm annualy, notably influenced by temperature, increasing by 28% at 240 °C. 2205 steel's yield strength decreases by 68 MPa with increasing temperature. The P110 steel consistently demonstrates superior characteristics, boasting the highest yield strength and lowest corrosion rate across different temperatures.

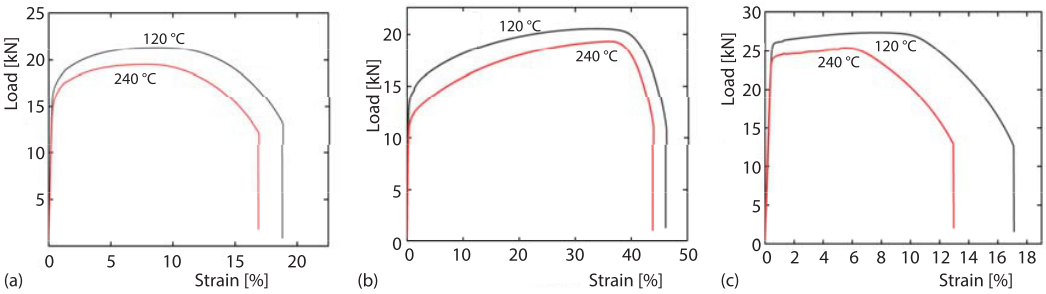

Figure 4. Stress-strain curves of materials at different temperatures; (a) load-strain curve of L80, (b) load-strain curve of 2205, and (c) load-strain curve of P110

Table 5. Calculation results of high temperature elastic modulus for the three materials

Material	Elastic modulus at 120 °C [GPa]	Elastic modulus at 240 °C [GPa]
L80	198	192
2205	193	191
P110	195	191

Table 6. The calculated mechanical parameters of high temperature tensile testing for three types of materials

Material	Temperature [°C]	Yield strength [MPa]	Tensile strength [MPa]	Temperature [°C]	Yield strength [MPa]	Tensile strength [MPa]
L80	120	564	701	240	522	645
2205		431	670		363	628
P110		817	866		773	818

Conclusion

In the weight loss corrosion test, all three materials developed a dark brown corrosion layer, with the corrosion rate increasing notably with temperature. The L80 steel exhibited the highest average corrosion rate at 0.0513 mm annualy, varying significantly with temperature. Temperature had minimal impact on elastic modulus but affected yield and tensile strength inversely. For instance, P110 had the highest yield strength, while 2205 showed the lowest. However, at 240 °C, both strengths decreased while elongation after fracture increased. The L80's corrosion rate rose by 28% with temperature, while 2205's yield strength dropped by 68 MPa. Overall, P110 demonstrated superior characteristics, boasting the highest yield strength and the lowest corrosion rate across varying temperatures, making it a preferred choice for service environments.

References

[1] Wang, F., *et al.*, A Review on Carbon Dioxide Corrosion of Steel in Oilfield Exploitation, *Corrosion Science and Protection Technology*, *4* (2002), 2, pp. 223-226
[2] Zhang, Z., *et al*., Law of CO_2 Corrosion of Oil Country Tubular Goods and the Study of Its Progress at Home and Abroad, *Baosteel Technology*, *4* (2000), 1, pp. 54-58
[3] Liu, Z., *et al.*, *Evaluation Method for Corrosion Experiments of Typical Materials in Oil and Gas Fields*, Science Press, Beijing, China, 2016
[4] Wang, F., *et al.*, *Principles, Methods, and Applications of Corrosion Electrochemistry*, Chemical Industry Press, Beijing, China, 2008
[5] Zhou, W., *et al*., Corrosion Electrochemical Behavior of Zn-Al Silane Coating on Carbon Steel, *Acta Metallurgica Sinica*, *9* (2007), 2, pp. 983-988
[6] Han, S., *Metal Corrosion Microstructure Map*, National Defense Industry Press, Beijing, China, 2008

Paper submitted: March 24, 2024
Paper revised: March 29, 2024
Paper accepted: May 11, 2024